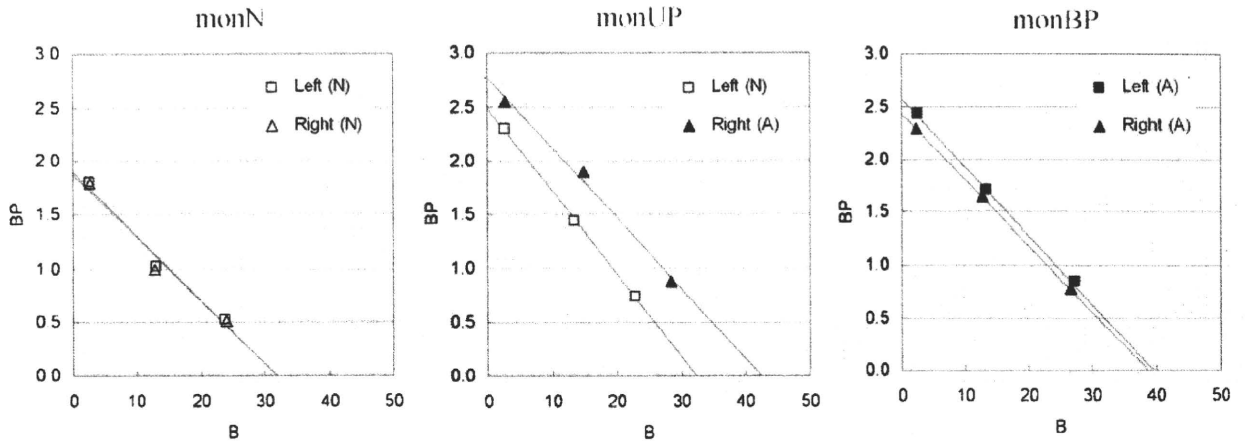

Figure 6 Single-scan, multiple-injection graphical analysis for normal (N) or affected (A) region of the left or right striatum in three monkeys that were normal (monN), unilateral Parkinsonian (monUP), and bilateral Parkinsonian (monBP).

Table 1 Estimated B_{max} and K_d values in three monkey studies

Scan protocol	*Subject*	*Region*	*Diagnosis*	B_{max} *(pmol/mL)*	K_d *(pmol/mL)*
Single scan	monN	L	N	31.8	16.7
		R	N	31.7	16.9
	monUP	L	N	32.3	13.0
		R	A	42.3	15.2
	monBP	L	A	39.6	15.4
		R	A	38.7	15.9
Three scans	monUP	L	N	29.2	11.6
		R	A	36.4	13.3

L, left striatum; R, right striatum; N, normal striatum; A, affected striatum.

left striatum. Both B_{max} and K_d of the single PET scan approach were slightly higher than those of the three PET scan approach. However, importantly, both approaches found that B_{max} in the affected striatum was higher than that in the normal striatum. The bilateral Parkinsonian animal showed B_{max} values of left = 39.6 pmol/mL, right = 38.7 pmol/mL, both of which were higher than those of the striatum of the normal animal or the normal striatum of the unilateral animal, but were very close to the affected striatum of the unilateral animal. The K_d values of the bilateral animal were not so different from other striatums.

Discussion

Density and Affinity Determination by Graphical Analysis with the Reference Region

In the graphical analysis for PET receptor studies, the values of B_{max} and K_d were estimated from the relationship between the ratio of bound to free concentrations and bound concentration at the time of transient equilibrium, using the TAC of the reference region (Farde *et al*, 1986). Some groups have used the value estimated from the distribution volume ratio − 1, instead of the B^{ref}/F^{ref} value of the y axis, because the values of B^{ref}/F^{ref} could change considerably with small changes in the time point of the transient equilibrium T_{eq} determined as the maximum C_b^{ref} (Logan *et al*, 1997; Doudet and Holden, 2003; Doudet *et al*, 2003). Distribution volume ratio or BP_{ND} is estimated from the kinetic analysis with TACs of target and reference regions, so it is not affected by the error of estimated T_{eq}. On the other hand, the value of $k'_3(t)$ in Equation (2) varies according to the concentration of bound raclopride, and estimates of BP_{ND} are considered to be an averaged value of specific binding over time, which is influenced by the dynamics of the free and bound raclopride. Despite this, in our simulation study of [^{11}C]raclopride, there was little difference between B^{ref}/F^{ref} and BP_{ND} estimated by the SRTM, and both had a linear correlation with B^{ref} (Figure 2). However, B^{ref}/F^{ref} became smaller than BP_{ND} and deviated from the linear relationship between B^{ref}/F^{ref} and B^{ref} in the region with low B^{ref} (Figure 2), especially for the TACs with high B_{max}. This may be a result of imperfect attainment of the transient equilibrium within the 50 mins scan duration for the TAC with high binding. There was little effect of the error of B^{ref} for the graphical analysis, in which B^{ref} varied widely among three injections, whereas the error of B^{ref}/F^{ref}

because of nonachievement of transient equilibrium had much effect on the graphical analysis as compared with BP_{ND}. Therefore, we estimated B_{max} and K_d by the graphical analysis with the relationship between BP_{ND} and B^{ref}.

In the simulations with various injected masses of [^{11}C]raclopride, it was shown that the relationship between BP_{ND} and B^{ref} became linear to some extent. However, BP_{ND} deviated from the linear relationship and approached a nonzero value when B^{ref} became larger (Figure 2). Therefore, in the B_{max} and K_d estimation by the graphical analysis with the reference TAC, points must be plotted within the range of the linear relation. As the relationship between BP_{ND} and B estimated from C_b using the plasma input function, without the reference TAC, remained linear even when B became large and the estimated BP_{ND} approached 0 (data not shown), this apparent saturation seemed to be owing to the reference region. Strictly speaking, the time course of free radioligand C_f is different from that of the reference region C_r (Figure 1) and C_f changes according to the specific binding that was affected by k_{on}, B_{max}, or administered mass of raclopride as pointed out by Ito *et al* (1998). Therefore, the time of the transient equilibrium estimated using C_b^{ref} was different from that estimated using C_b, and B^{ref} was often different as well. In addition, the value of BP_{ND} estimated by SRTM was lower than the BP_{ND} estimated from the two-tissue compartment model with the plasma input function.

This difference between the target and reference TAC affected the B_{max} and K_d estimates as well. In the simulated TACs with various B_{max} or K_d values, the B_{max} and K_d were overestimated compared with the true values even in the conventional three PET scan approach (Figure 3). On the other hand, the overestimation was not observed when B_{max} and K_d were estimated by the graphical analysis using C_f and C_b without the reference TAC (Figure 3), demonstrating that graphical analysis could determine B_{max} and K_d precisely if C_b were obtained correctly. However, the free and bound concentrations in the target region cannot be distinguished from the total concentration measured by PET scanning without arterial blood sampling, and in practical PET data, estimation of rate constants with the plasma input function is unstable and impractical. Therefore, in the usual graphical analysis, the TAC of reference region is used as the free radioligand concentration in the target region (Farde *et al*, 1989). The effect of the reference TAC on B_{max} and K_d estimates depends on the kinetics of the tracer in each region, which depends in turn on the particular tracers and species. In the simulated TACs of monkeys with [^{11}C]raclopride, there was a good correlation between true and estimated K_d or B_{max}, though estimates were biased. Therefore, we concluded the graphical analysis with reference TAC is practical for [^{11}C]raclopride studies, because it can detect the value of B_{max} or K_d in neurological or psychiatric disorders without arterial blood sampling.

Estimated Density and Affinity by the Multiple-Injection Approach

We applied the multiple-injection approach to the graphical analysis for B_{max} and K_d determination in an effort to shorten the total duration of the scanning protocol, and to obviate the need for several radiosyntheses for each animal. From the relationship between the BP_{ND} estimates and injected mass in the simulation study (Figure 2), the molar amounts of three injections were set as 1.5, 10, and 30 nmol/kg, so that the estimated BP_{ND} would be high, intermediate, and low within the range in which the linear correlation held. The injection interval was set to 50 mins, because it has been reported in monkey studies that 50 mins scan duration could provide reliable BP_{ND} estimates even for TACs with high and low BP_{ND} values (Ikoma *et al*, 2009). In our present studies on monkeys with this protocol, injected masses increased with each successive injection, but amounts of administered radioactivity remained fairly constant, i.e., 57, 60, and 31 MBq. Therefore, the signal to noise ratio of image quality did not change seriously for each injection.

In the usual graphical analysis by nonsequential multiple PET scans, the molar amount of administered [^{11}C]raclopride for each scan is adjusted by varying the specific activity of administered [^{11}C]raclopride. Several investigators have attempted to perform multiple injections of ligands with PET studies to obtain receptor density and affinity by changing specific activity with a detailed model equation (Delforge *et al*, 1995; Millet *et al*, 1995; Morris *et al*, 1996; Muzic *et al*, 1996; Christian *et al*, 2004; Gallezot *et al*, 2008). Meanwhile, our approach requires only one synthesis of [^{11}C]raclopride, which is split to three with different mass of raclopride with same specific activity. By keeping the specific activity throughout scan, we can directly interpret PET counts in pmol/mL unit.

In the simulations of B_{max} and K_d estimation with this single PET scan approach, B_{max} and K_d were overestimated compared with the true values, just as seen in the three PET scan approach. Furthermore, estimates of both parameters were higher than those in the three PET scan approach. In the single PET scan approach, the error because of assumptions of the reference tissue approach could be more severe than for the three PET scan approach, because the residual radioactivities at the times of the second and third injections could propagate to error of B^{ref} or BP_{ND} estimates. This was shown to be the case in the simulation study, in which the relationship between the BP_{ND} and B^{ref} in the third injection was a little different from that in the first injection (Figure 2). Furthermore, our approach assumes that BP_{ND} is promptly altered by the next injection, but this is in fact not exactly the case. We showed the bias of the estimated BP_{ND} related to this assumption (Ikoma *et al*, 2009), and the estimated B_{max} and K_d in this paper consequently could be biased. However, in the

simulations, B_{max} and K_d estimated by the MI-GA changed according to the variation of the true values (Figure 3), demonstrating this approach could be applied to the quantitative evaluation of B_{max} and K_d from a single session of PET scanning.

Monkey Studies

In the simulations, we demonstrated that the MI-GA could detect density and affinity of dopamine D_2 receptors. Furthermore, we demonstrated the validity of the proposed method using actual data from monkeys. As a result, the three BP_{ND} data points calculated from the single PET scan with three sequential injections of different administration masses were almost on a straight line, and estimated values of B_{max} and K_d were very close to those previously obtained *in vitro* ($B_{max} = 25.7$ pmol/g) (Madras *et al*, 1988) or *in vivo* by the conventional method in monkeys ($B_{max} = 22$ pmol/mL, $K_d = 13.5$ nmol/L) (Doudet *et al*, 2003). The estimates by the single PET scan approach were slightly higher than those by the three PET scan approach, and this was consistent with the results from the current simulations.

Although we investigated only three monkeys in this study, the values of B_{max} in the partially denervated striata was higher than in normal striatum, whereas the apparent affinity was unaffected by the MPTP lesions. Likewise Rinne *et al* (1995) reported a 35% increase in the D_2 B_{max} in the putamen contralateral to the side of predominant motor symptoms, without any discernible effect on apparent affinity. In our monkey measurements, in the hemilesioned monkey, the B_{max} was elevated by 31% on the denervated side. In the animal with bilateral MPTP lesion, the B_{max} in both striata was higher than in the normal animal, or in the unlesioned side of the hemiparkinsonian animal, despite no significant changes in K_d values: the results were consistent with those of the previous report.

In addition to the results of ROI analysis, which disclosed bulk D_2 receptor characteristics in the whole striatum, parametric imaging of B_{max} and K_d (as shown in Figure 5) suggested a potential significance in regional estimation of D_2 receptor characteristics. Although ROI analysis disclosed higher B_{max} values in the MPTP-infused side of the striatum, the parametric imaging showed the increase of B_{max} was more evident in the dorsal and posterior parts of the striatum. A similar finding of preferential lesion in dorsal and posterior parts of the striatum has been reported based on neurochemical and pathological assessments of MPTP-lesioned monkeys (Oiwa *et al*, 2003). As the current parametric imaging may have significant artifacts, such as those arising from low signal-to-noise ratio, partial volume effects, small number of points, the situation should be improved through the use of a higher resolution PET scanner.

Potential Limitations of the Multiple-Injection Graphical Analysis

The multiple-injection approach is able to assess the B_{max} and K_d for receptor studies in a single PET scan with single radiosynthesis, and shortened study period as compared with a conventional approach. This approach might also be applicable to other PET ligands and receptor types, but with several caveats: First, it is necessary to evaluate whether the reference region can be used as the free TAC of the target region. The kinetics of the target and reference regions is affected by the value of each rate constant, i.e., K_1, k_2, B_{max}, and K_d, that differ between species and radioligands. The difference between C_{ref} and C_f often causes an error in B^{ref}, and the estimated B_{max} and K_d should be interpreted with caution when the reference region has considerably different kinetics. Second, the molar amounts of administered ligand need to be selected such that the resultant BP_{ND} will be within the range in which the linear relationship between BP_{ND} and B holds. In the case of regions with low BP_{ND}, and small extent of the necessary linear relationship, it may be difficult to determine B_{max} and K_d reliably. Third, the interval of three injections should be determined so that the free ligand TAC has a transient equilibrium within the scan duration of each injection, especially when the injected mass is small, i.e., BP_{ND} is high. The radioligand [^{11}C]raclopride dissociates rapidly from the receptors, allowing equilibration of binding to be established *in vivo* within the time span of PET experiments (Farde *et al*, 1989; Ito *et al*, 1998). However, those ligands with slow kinetics, such as [^{18}F]fallypride require a longer scan duration such that the present graphical analysis may not be suitable in all instances. Despite these limitations, by optimizing the administered mass and the time interval between three injections of [^{11}C]raclopride, we have shown that the multiple-injection approach can determine B_{max} and K_d values as effectively as an approach using three separate scans, but within a single scan time of 150 mins.

Moreover, the bias of B_{max} and K_d estimated by the single scan approach with two injections was not larger than that by the single scan approach with three injections in the simulations (data not shown), and points of the second and third injections in MI-GA were almost on the same line in the monkey studies (Figure 6). Therefore, there is a possibility of reducing scan time and exposure further using only two injections, though the effect of statistical noise on estimates should be considered.

Conclusion

We developed the method for estimating B_{max} and K_d values in a single session of PET scanning with multiple injections of [^{11}C]raclopride. Our simulations showed that the MI-GA could detect B_{max} and K_d values by using the optimal injection protocol. We

also demonstrated in monkey studies that B_{max} and K_d values estimated by our proposed approach were proper compared with previous monkey studies or our studies by the conventional method. The proposed method made it possible to determine the dopamine D_2 receptor density and affinity by a 150 mins PET scan with three injections of [^{11}C]raclopride at 50 mins intervals.

Acknowledgements

We thank Dr Jun Takahashi (Kyoto University) for providing us animals for this study. This research was supported by the Ministry of Education, Culture, Sports, Science and Technology of Japan (MEXT) grant-in-aid for Young Scientists (B) (No. 20790839), grant-in-aid for Scientific Research (C) (No. 09019855) (TH), Kobe Cluster I and II, and the Ministry of Health, Labour, and Welfare of Japan (MHLW) Health Science Research Grant, H17-025 (TH, HI). We are grateful to members of Department of Investigative Radiology, National Cardiovascular Center Research Institute, for their support of PET experiment and for helpful suggestions.

Conflict of interest

The authors declare no conflict of interest.

References

Bankiewicz KS, Oldfield EH, Chiueh CC, Doppman JL, Jacobowitz DM, Kopin IJ (1986) Hemiparkinsonism in monkeys after unilateral internal carotid artery infusion of 1-methyl-4-phenyl-1,2,3,6-tetrahydropyridine (MPTP). *Life Sci* 39:7–16

Christian BT, Narayanan T, Shi B, Morris ED, Mantil J, Mukherjee J (2004) Measuring the *in vivo* binding parameters of [^{18}F]-fallypride in monkeys using a PET multiple-injection protocol. *J Cereb Blood Flow Metab* 24:309–22

Cross AJ, Crow TJ, Owen F (1981) ^{3}H-Flupenthixol binding in post-mortem brains of schizophrenics: evidence for a selective increase in dopamine D2 receptors. *Psychopharmacology (Berl)* 74:122–4

Delforge J, Pappata S, Millet P, Samson Y, Bendriem B, Jobert A, Crouzel C, Syrota A (1995) Quantification of benzodiazepine receptors in human brain using PET, [^{11}C]flumazenil, and a single-experiment protocol. *J Cereb Blood Flow Metab* 15:284–300

Doudet DJ, Holden JE (2003) Sequential versus non-sequential measurement of density and affinity of dopamine D_2 receptors with [^{11}C]raclopride: Effect of methamphetamine. *J Cereb Blood Flow Metab* 23:1489–94

Doudet DJ, Jivan S, Holden JE (2003) *In vivo* measurement of receptor density and affinity: comparison of the routine sequential method with a nonsequential method in studies of dopamine D_2 receptors with [^{11}C]raclopride. *J Cereb Blood Flow Metab* 23:280–4

Farde L, Ehrin E, Eriksson L, Greitz T, Hall H, Hedström CG, Litton JE, Sedvall G (1985) Substituted benzamides as ligands for visualization of dopamine receptor binding in the human brain by positron emission tomography. *Proc Natl Acad Sci USA* 82:3863–7

Farde L, Eriksson L, Blomquist G, Halldin C (1989) Kinetic analysis of central [^{11}C]raclopride binding to D_2-dopamine receptors studied by PET — A comparison to equilibrium analysis. *J Cereb Blood Flow Metab* 9: 696–708

Farde L, Hall H, Ehrin E, Sedvall G (1986) Quantitative analysis of D_2 dopamine receptor binding in the living human brain by PET. *Science* 231:258–61

Farde L, Wiesel FA, Hall H, Halldin C, Stone-Elander S, Sedvall G (1987) No D_2 receptor increase in PET study of schizophrenia. *Arch Gen Psychiatry* 44:671–2

Farde L, Wiesel FA, Stone-Elander S, Halldin C, Nordström AL, Hall H, Sedvall G (1990) D_2 dopamine receptors in neuroleptic-naive schizophrenic patients. A positron emission tomography study with [^{11}C]raclopride. *Arch Gen Psychiatry* 47:213–9

Gallezot JD, Bottlaender MA, Delforge J, Valette H, Saba W, Dollé F, Coulon CM, Ottaviani MP, Hinnen F, Syrota A, Grégoire MC (2008) Quantification of cerebral nicotinic acetylcholine receptors by PET using 2-[^{18}F]fluoro-A-85380 and the multiinjection approach. *J Cereb Blood Flow Metab* 28:172–89

Gunn RN, Lammertsma AA, Hume SP, Cunningham VJ (1997) Parametric imaging of ligand-receptor binding in PET using a simplified reference region model. *Neuroimage* 6:279–87

Guttman M, Seeman P (1985) L-dopa reverses the elevated density of D_2 dopamine receptors in Parkinson's diseased striatum. *J Neural Transm* 64:93–103

Hall H, Köhler C, Gawell L, Farde L, Sedvall G (1988) Raclopride, a new selective ligand for the dopamine-D_2 receptors. *Prog Neuropsychopharmacol Biol Psychiatry* 12:559–68

Herzog H, Tellmann L, Hocke C, Pietrzyk U, Casey ME, Kuwert T (2004) NEMA NU2-2001 guided performance evaluation of four Siemens ECAT PET scanners. *IEEE Trans Nucl Science* 51:2662–9

Ikoma Y, Watabe H, Hayashi T, Miyake Y, Teramoto N, Minato K, Iida H (2009) Quantitative evaluation of changes in binding potential with a simplified reference tissue model and multiple injections of [^{11}C]raclopride. *Neuroimage* 47:1639–48

Ito H, Hietala J, Blomqvist G, Halldin C, Farde L (1998) Comparison of the transient equilibrium and continuous infusion method for quantitative PET analysis of [^{11}C]raclopride binding. *J Cereb Blood Flow Metab* 18:941–50

Joyce JN, Lexow N, Bird E, Winokur A (1988) Organization of dopamine D_1 and D_2 receptors in human striatum: receptor autoradiographic studies in Huntington's disease and schizophrenia. *Synapse* 2:546–57

Köhler C, Hall H, Ogren SO, Gawell L (1985) Specific *in vitro* and *in vivo* binding of ^{3}H-raclopride. A potent substituted benzamide drug with high affinity for dopamine D-2 receptors in the rat brain. *Biochem Pharmacol* 34:2251–9

Lammertsma AA, Hume SP (1996) Simplified reference tissue model for PET receptor studies. *Neuroimage* 4:153–8

Logan J, Fowler JS, Volkow ND, Wang GJ, Ding YS, Alexoff DL (1996) Distribution volume ratios without blood sampling from graphical analysis of PET data. *J Cereb Blood Flow Metab* 16:834–40

Logan J, Volkow ND, Fowler JS, Wang GJ, Fischman MW, Foltin RW, Abumard NN, Vitkun S, Gatley SJ, Pappas N, Hitzemann R, Shea CE (1997) Concentration and occupancy of dopamine transporters in cocaine abusers with [^{11}C]cocaine and PET. *Synapse* 27:347–56

Madras BK, Fahey MA, Canfield DR, Spealman RD (1988) D1 and D2 dopamine receptors in caudate-putamen of nonhuman primates (*macaca fascicularis*). *J Neurochem* 51:934–43

Millet P, Delforge J, Mauguiere F, Pappata S, Cinotti L, Frouin V, Samson Y, Bendriem B, Syrota A (1995) Parameter and index images of benzodiazepine receptor concentration in the brain. *J Nucl Med* 36:1462–71

Mintun MA, Raichle ME, Kilbourn MR, Wooten GF, Welch MJ (1984) A Quantitative model for the *in vivo* assessment of drug binding sites with positron emission tomography. *Ann Neurol* 15:217–27

Morris ED, Babich JW, Alpert NM, Bonab AA, Livni E, Weise S, Hsu H, Christian BT, Madras BK, Fischman AJ (1996) Quantification of dopamine transporter density in monkeys by dynamic PET imaging of multiple injections of ^{11}C-CFT. *Synapse* 24:262–72

Muzic RR, Nelson AD, Saidel GM, Miraldi F (1996) Optimal experiment design for PET quantification of receptor concentration. *IEEE Trans Med Imaging* 15:2–12

Oiwa Y, Eberling JL, Nagy D, Pivirotto P, Emborg ME, Bankiewicz KS (2003) Overlesioned hemiparkinsonian non human primate model: correlation between clinical, neurochemical and histochemical changes. *Front Biosci* 8:155–66

Rinne JO, Laihinen A, Ruottinen H, Ruotsalainen U, Någren K, Lehikoinen P, Oikonen V, Rinne UK (1995) Increased density of dopamine D_2 receptors in the putamen, but not in the caudate nucleus in early Parkinson's disease: a PET study with [^{11}C]raclopride. *J Neurol Sci* 132:156–61

Scatchard G (1949) The attractions of proteins for small molecules and ions. *Ann NY Acad Sci* 51:660–72

Seeman P, Bzowej NH, Guan HC, Bergeron C, Reynolds GP, Bird ED, Riederer P, Jellinger K, Tourtellotte WW (1987) Human brain D_1 and D_2 dopamine receptors in schizophrenia, Alzheimer's, Parkinson's, and Huntington's diseases. *Neuropsychopharmacology* 1:5–15

Takagi Y, Takahashi J, Saiki H, Morizane A, Hayashi T, Kishi Y, Fukuda H, Okamoto Y, Koyanagi M, Ideguchi M, Hayashi H, Imazato T, Kawasaki H, Suemori H, Omachi S, Iida H, Itoh N, Nakatsuji N, Sasai Y, Hashimoto N (2005) Dopaminergic neurons generated from monkey embryonic stem cells function in a Parkinson primate model. *J Clin Invest* 115:102–9

Watabe H, Ohta Y, Teramoto N, Miyake Y, Kurokawa M, Yamamoto A, Ose Y, Hayashi T, Iida H (2006) A novel reference tissue approach for multiple injections of [C-11]Raclopride. *Neuroimage* 31:T73

Wong DF, Wagner Jr HN, Tune LE, Dannals RF, Pearlson GD, Links JM, Tamminga CA, Broussolle EP, Ravert HT, Wilson AA, Toung JK, Malat J, Williams JA, O'Tuama LA, Snyder SH, Kuhar MJ, Gjedde A (1986) Positron emission tomography reveals elevated D_2 dopamine receptors in drug-naive schizophrenics. *Science* 234:1558–63

Appendix

The multiple-injection two-tissue four-parameter compartment model is based on the following differential equations:

$$\frac{dC_f}{dt} = K_1 C_p(t) - (k_2 + k_3) C_f(t) + k_4 C_b(t) \qquad (A1)$$

$$\frac{dC_b}{dt} = k_3 C_f(t) - k_4 C_b(t) \qquad (A2)$$

where C_p is the radioactivity concentration of metabolite-corrected plasma, C_f and C_b are the concentrations of radioactivity for free and specifically bound ligand in tissue, respectively.

Equations (A1) and (A2) are solved with the radioactivity concentration of C_f and C_b at the time of injection, that is $C_f(0)$ and $C_b(0)$, then $C_f(t)$, $C_b(t)$ and total radioactivity concentration in tissue $C_t(t)$ are expressed as following equations:

$$\begin{aligned} C_f(t) = {} & \frac{K_1}{\alpha_2 - \alpha_1}\{(k_4 - \alpha_1)e^{-\alpha_1 t} - (k_4 - \alpha_2)e^{-\alpha_2 t}\} \otimes C_p(t) \\ & + \frac{1}{\alpha_2 - \alpha_1}\{(k_4 - \alpha_1)C_f(0) + k_4 C_b(0)\}e^{-\alpha_1 t} \\ & - \frac{1}{\alpha_2 - \alpha_1}\{(k_4 - \alpha_2)C_f(0) + k_4 C_b(0)\}e^{-\alpha_2 t} \end{aligned} \qquad (A3)$$

$$\begin{aligned} C_b(t) = {} & \frac{K_1 k_3}{\alpha_2 - \alpha_1}\left(e^{-\alpha_1 t} - e^{-\alpha_2 t}\right) \\ & \otimes C_p(t) + \frac{k_3}{\alpha_2 - \alpha_1}\left(C_f(0) + \frac{k_4}{k_4 - \alpha_1} C_b(0)\right)e^{-\alpha_1 t} \\ & - \frac{k_3}{\alpha_2 - \alpha_1}\left(C_f(0) + \frac{k_4}{k_4 - \alpha_2} C_b(0)\right)e^{-\alpha_2 t} \\ & + \left(\frac{k_3 k_4}{(k_4 - \alpha_1)(k_4 - \alpha_2)} + 1\right) C_b(0) e^{-k_4 t} \end{aligned} \qquad (A4)$$

$$\begin{aligned} C_t(t) = {} & \frac{K_1}{\alpha_2 - \alpha_1}\{(k_3 + k_4 - \alpha_1)e^{-\alpha_1 t} - (k_3 + k_4 - \alpha_2)e^{-\alpha_2 t}\} \\ & \otimes C_p(t) + \frac{k_3 + k_4 - \alpha_1}{\alpha_2 - \alpha_1}\left(C_f(0) + \frac{k_4}{k_4 - \alpha_1} C_b(0)\right)e^{-\alpha_1 t} \\ & - \frac{k_3 + k_4 - \alpha_2}{\alpha_2 - \alpha_1}\left(C_f(0) + \frac{k_4}{k_4 - \alpha_2} C_b(0)\right)e^{-\alpha_2 t} \\ & + \left(\frac{k_3 k_4}{(k_4 - \alpha_1)(k_4 - \alpha_2)} + 1\right) C_b(0) e^{-k_4 t} \\ \alpha_{1,2} = {} & \frac{(k_2 + k_3 + k_4) \mp \sqrt{(k_2 + k_3 + k_4)^2 - 4k_2 k_4}}{2} \end{aligned} \qquad (A5)$$

3-Tesla Magnetic Resonance Angiographic Assessment of a Tissue-Engineered Small-Caliber Vascular Graft Implanted in a Rat

Masashi Yamanami,[1,2] Akihide Yamamoto,[3,4] Hidehiro Iida,[3,4] Taiji Watanabe,[1,2] Keiichi Kanda,[2] Hitoshi Yaku,[2] Yasuhide Nakayama[1]

[1] Department of Bioengineering, Advanced Biomedical Engineering Center, National Cardiovascular Center Research Institute, Osaka, Japan

[2] Department of Cardiovascular Surgery, Kyoto Prefectural University of Medicine, Kyoto, Japan

[3] Department of Investigative Radiology, Advanced Biomedical Engineering Center, National Cardiovascular Center Research Institute, Osaka, Japan

[4] Department of Medical Physics and Engineering, Division of Health Sciences, Graduate School of Medicine, Osaka University, Osaka, Japan

Received 30 January 2009; revised 4 June 2009; accepted 15 July 2009
Published online 2 October 2009 in Wiley InterScience (www.interscience.wiley.com). DOI: 10.1002/jbm.b.31501

Abstract: In the development of small-caliber vascular grafts (diameter; less than 3 mm), animal implantation studies have been mostly performed by using rat abdominal aortas, and their certain patency must evaluate with sacrificing every observation periods, which is both labor-intensive and time-consuming when performing a large number of experiments. This study is the first to demonstrate the application of 3-Tesla contrast-free time-of-flight magnetic resonance angiography (TOF-MRA) in the continuous assessment of the status of a tissue-engineered vascular graft in rat. As a model graft, a single connective tubular tissue (diameter; 1.5 mm), prepared by embedding the silicone rod (diameter; 1.5 mm) into a subcutaneous pouch of a rat for 2 weeks an *in vivo* tissue-engineering, was used. The graft was implanted in the abdominal aorta (diameter; 1.3 mm) of the rat by end-to-end anastomosis. Repeated TOF-MRA imaging of the graft obtained over a 3-month follow-up period after implantation made it possible to evaluate the patency of the graft, both simply and noninvasively. It also permitted visualization of the connected abdominal aorta and renal and common iliac arteries having smaller caliber (diameter; less than 1 mm). In addition, the degree of the stenosis or aneurysm could also be detected. 3-Tesla MRA allowed the simplified and noninvasive assessment of the status on the vascular graft, including the formation of a stenosis or aneurysm, in the same rat at different times, which will be contributing to enhance the development of tissue-engineered vascular grafts even with small caliber. © 2009 Wiley Periodicals, Inc. J Biomed Mater Res Part B: Appl Biomater 92B: 156–160, 2010

Keywords: small-caliber vascular grafts; magnetic resonance angiography; animal implantation; biotube; tissue engineering

INTRODUCTION

Small-caliber arterial substitutes are needed for cardiac and peripheral revascularization procedures. For such small artery bypass grafting procedures, autologous arterial (e.g., internal thoracic artery and radial artery) or venous (e.g., saphenous vein) grafts still remain the most ideal vascular substitutes.[1,2] However, many patients do not have a vessel suitable for use owing to the poor quality, inadequate size or length, or previous harvest of such vessels. Moreover, a second surgical procedure is required to initially obtain the necessary vessel. Vascular prostheses, such as expanded polytetrafluoroethylene (ePTFE) and poly (ethylene terephthalate) (Dacron) grafts, have been used clinically for reconstructing arteries.[3] However, small-caliber (<6 mm) arterial substitutes have generally proved inadequate largely because of the formation of thromboses and intimal hyperplasia.[4,5]

Many design criteria have been proposed for the development of functional small-caliber arterial replacement grafts.[5–11] All most of all artificial vascular grafts (inner diameter, 1.5–3.0 mm) have been employed for transplantation

Correspondence to: Y. Nakayama (e-mail: nakayama@ri.ncvc.go.jp)

to rat abdominal aortas as an *in vivo* model.[6–8] Graft patency has been evaluated during the follow-up period by angiography[8] or by direct inspection at the time of removal for histological evaluation.[6,7] However, angiography requires cannulation of the carotid artery,[8] and a midline laparotomy is needed for direct inspection.[6,7] As a consequence, these methods are complex and invasive. Therefore, it is difficult to evaluate graft patency repeatedly in the same rat. Although, graft patency has also been evaluated by palpating the femoral pulse,[7] this method is subjective and uncertain.

The current imaging systems, including fluorescence antibody method, single photon emission computed tomography (SPECT),[12] laser doppler system,[13] or high-resolution ultrasound[14] for blood flow imaging in addition to magnetic resonance angiography (MRA), are powerful tool in tissue engineering field. However, it is considered that no imaging systems except for MRA fit for evaluation of the status of implanted small-caliber vascular grafts.

In clinical practice, MRI has been used as a noninvasive evaluation method for the assessment of brain blood vessels and peripheral arteries and also been widely used in preclinical research on experimental small rodents.[15–18] The studies have typically been aimed at understanding the patho-physiological status and evaluating the efficacy/side effects of newly developed treatments, such as pharmaceutical and regenerative medicine.

Our purpose in this study was to evaluate the status of a tissue-engineered vascular graft with inner diameter of 1.5 mm, clinically, repeatedly, and noninvasively in a rat implantation model. To this end, 3-Tesla contrast-free time-of-flight magnetic resonance angiography (TOF-MRA) was applied.

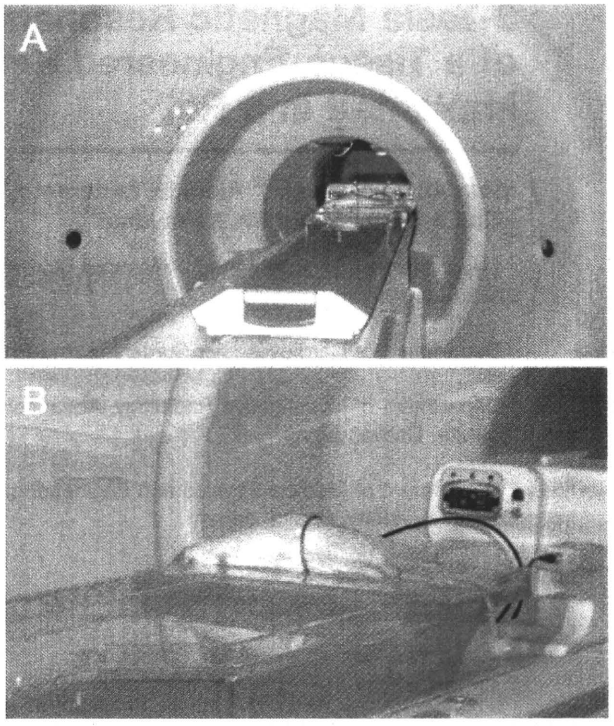

Figure 1. Experimental setup in MR imaging on a human whole-body 3T-MR scanner (GE Healthcare) (A). The coil was placed at the center of the gantry and its turn axis had perpendicular alignment to the static magnetic field (B). Rat's abdomen was positioned inside the coil along the craniocaudal direction. [Color figure can be viewed in the online issue, which is available at www.interscience.wiley.com.]

MATERIALS AND METHODS

Preparation and Implantation of the Connective Tubular Tissue

All animal experiments were conducted in accordance with local regulations, complying with the Principles of Laboratory Animal Care (formulated by the National Society for Medical Research) and the Guide for the Care and Use of Laboratory Animals (NIH Publication No. 86–23, revised 1985). The research protocol (No. 8050) was approved by the ethics committee of the National Cardiovascular Center Research Institute.

The connective tubular tissue was prepared by *in vivo* tissue engineering according to the previous reported method.[9] Briefly, a silicone rod (diameter, 1.5 mm; length, 10 mm; Tigers Polymer, Osaka, Japan) was used as a mold. One adult female Wistar rat (weight; 300 g) was anesthetized with 1.5% isoflurane (vol/vol air). The mold was placed in a dorsal subcutaneous pouch, and after 2 weeks, the implant was removed. The tubular tissue was obtained from the implant after trimming the peripheral tissues and pulling out the rod. The tube thus obtained was treated by coating with Argatroban (1 mg/graft; Mitsubishi Chemical Co., Tokyo, Japan) to make it antithrombogenic. It was then implanted to the infrarenal abdominal aorta of the same rat using an end-to-end anastomosis under microscopic guidance and sutured using 12 interrupted 10–0 nylon stitches [Figure 1(A)]. Patency was examined at the time of surgery by direct inspection. The wound was closed with 4–0 silk sutures. Thereafter, the rat had free access to standard food and water. Graft status was evaluated at 2, 36, and 78 days after transplantation by contrast-free TOF-MRA under anesthesia induced by an intramuscular injection of pentobarbital (40 mg/kg).

MR Data Acqusition

A human whole-body 3-Tesla magnetic resonance imaging (MRI) scanner (Signa, GE Healthcare, Milwaukee, WI) was employed in this study (Figure 1). The gradient coil system was capable of providing a maximum gradient amplitude of 40 mT/m. All sequence programs employed in this study were designed for clinical studies. A developed single-turn surface coil of 62 mm diameter was used for MR imaging [Figure 1(B)]. Contrast-free TOF-MRA was performed using a three-dimensional flow-compensated fast spoiled gradient recalled (3D-FSPGR) sequence [repetition

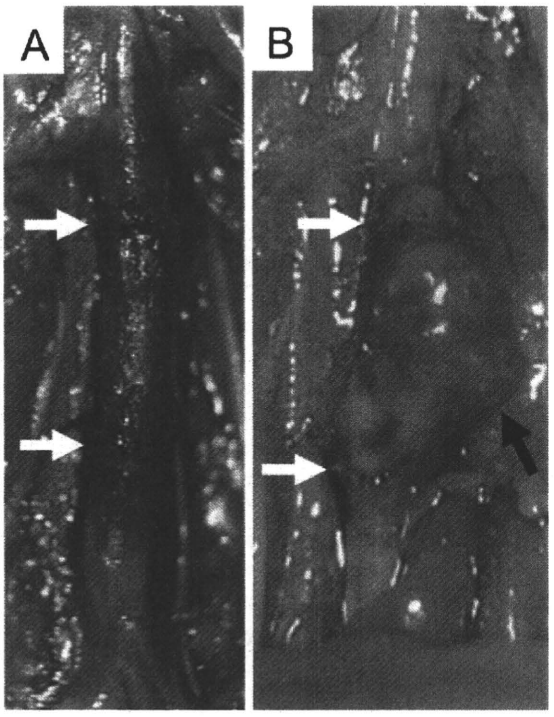

Figure 2. (A) The tubular connective tissue vascular graft (diameter; 1.5 mm) after autoimplantation in the rat infrarenal abdominal aorta (diameter; 1.3 mm) performed by end-to-end anastomosis under microscopic guidance using 12 interrupted stitches of 10-0 nylon suture. (B) The tubular connective tissue formed an aneurysm (max diameter; 3.0 mm) at 78 days after autoimplantation. White arrows indicate the proximal and distal anastomosis regions. Black arrow indicates the aneurysm. [Color figure can be viewed in the online issue, which is available at www.interscience.wiley.com.]

time (TR) = 21 ms, echo time (TE) = 5.4 ms (out of phase), flip angle (FA) = 15°, slice thickness = 0.4 mm, field of view (FOV) = 80 mm × 60 mm, matrix = 288 × 192, locs per slab = 128, the number of excitations (NEX) = 1, scanning time = 5 min 58 s]. For suppressing venous signals, a region of 40-mm thickness on the caudal side of the measured slab was saturated. The measured voxel size in TOF-MRA was 0.278 × 0.291 × 0.400 mm. The image reconstruction was zero-filled to a matrix size of 512 × 512 and the voxel size was 0.156 × 0.156 × 0.400 mm. MR angiograms were analyzed by generating the partial maximum intensity projection (pMIP) with a commercial software package (AZE, Tokyo, Japan). Our previous report on TOF-MRA was shown detail in rat.[13]

RESULTS

The tubular connective tissue with a diameter of 1.5 mm was autoimplanted successfully into the 1.3 mm diameter abdominal aorta of the rat by end-to-end anastomosis [Figure 2(A)]. After suturing with 12 interrupted stitches, there was little bleeding from either of the sites of anastomosis, indicated by the arrows in Figure 2(A). The patency of the graft was recognized directly by the satisfactory pulsation at the graft and distal side of the aorta.

3-Tesla contrast-free TOF-MRA of the rat was performed at 2 days after implantation [Figure 3(A)] to evaluate the status of the graft. The measurement time was ~6 min and no contrast medium was needed. The MRA distinctly visualized the patent graft connected to the abdominal aorta together with renal arteries and common iliac arteries of 0.7 and 0.8 mm diameter, respectively. Spatial resolution in the MRA was less than several hundred microns. A mechanical stenotic lesion, which may have been due to the anastomosis, was observed in both anastomosis regions. At 36 days after implantation, little stenosis and no aneurismal dilation of the graft were observed [Figure 3(B)]. At 78 days after implantation, the maximum diameter of the aneurysm formed at the graft was 3.0 mm [Figure 3(C)]. The shape of the aneurysm was very close to that observed macroscopically [Figure 2(B)]. Therefore, the status of the graft could be precisely determined, repeatedly, and noninvasively.

DISCUSSION

This study is the first to demonstrate the application of MRA to the evaluation of the status of a small-caliber arti-

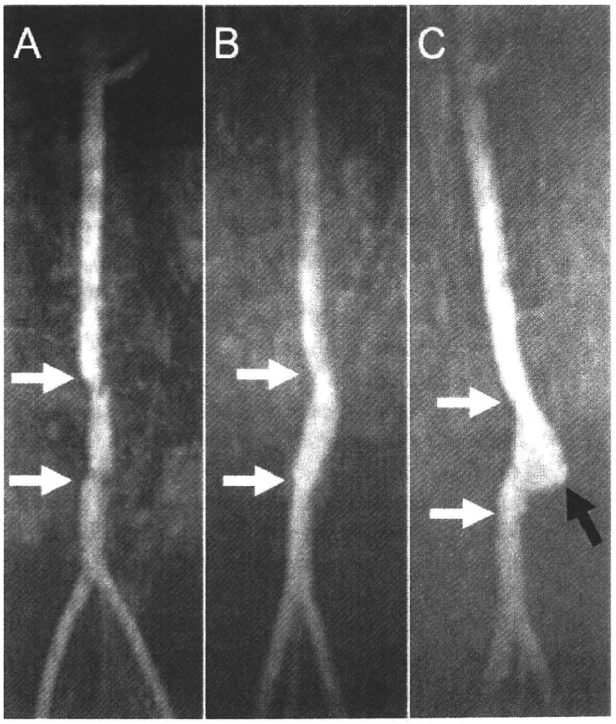

Figure 3. 3-Tesla contrast-free TOF-MRA images of the rat abdominal aorta at 2 (A), 36 (B), and 78 (C) days after autoimplantation of the biotube vascular graft. White arrows indicate the proximal and distal anastomosis regions of the abdominal aorta. A stenotic lesion was visible in the anastomosis regions at 2 days. An aneurysm formation in the graft was visible at 78 days (black arrow indicates the aneurysm).

ficial vascular graft implanted in the abdominal aorta of a rat. In the development of small-caliber vascular grafts as a preclinical study, *in vivo* evaluation is needed. Implantation studies have been performed mostly by using the abdominal aorta of rats.[6–8] Their certain patency must evaluate with sacrificing every observation periods, which is both labor-intensive and time-consuming when performing a large number of experiments. Since some rats survive with no symptoms after graft occlusion, assessment of the occlusion of an abdominal aorta after graft implantation is not possible solely on the basis of the rat's appearance. On the other hand, some researchers have evaluated graft patency by palpating the femoral pulse[7]; however, this method is prone to subjectivity and uncertainty. Therefore, evaluation of graft patency should be performed by direct inspection under laparotomy. On the other hand, even in histological observations, the evaluation of the degree of graft stenosis is very difficult.

In this study, MRI images of a reasonable quality were obtained from a rat using a human whole-body MRI scanner at 3-Tesla. Contrast-free TOF-MRA was able to depict the implanted graft with a diameter of ~1.5 mm, connected to the abdominal aorta with a diameter of ~1.3 mm, and also revealed arteries with diameters of less than 1 mm, such as the renal, common iliac, and tail arteries. In addition, an evaluation of the graft status, including the stenosis, was also feasible due to the high resolution and reasonable contrast. As indicated in Figure 3(A), the mechanical stenosis was clearly indicated at both sites of anastomosis. Furthermore, the aneurysm formation was clearly observed [Figure 3(C)]. Since the observation by MRA is simple and noninvasive, assessment of the status of small-caliber vascular grafts could be performed in the same rat at different times. The repeatable MRA observation in a single rat enabled correct assessment of the graft status over the follow-up period. Such repeatability will reduce the variation in results stemming from individual difference in experimental animals.

As a model graft for implantation in this study, the tubular connective tissue was used. The tissue was prepared similar to biotubes.[9] Biotubes are autologous prosthetic tubular tissues prepared by in-body tissue architecture technology. The biotube, obtained from rats by embedding the silicone rods (diameter; 3 mm) into their subcutaneous pouches for 4 weeks, had several 10 μm in thickness, about 500 gf in maximum load at rapture, and about 1000 mmHg in burst pressure.[19] This technology, a novel and practical concept in regenerative medicine, is based on the phenomenon of tissue encapsulation of foreign materials *in vivo*, and it can be used to develop autologous tissues of the desired shape, depending on the mold design.[9–11] Using this technology, several types of tissues, including "biotubes" as vascular tissues,[9–11] "biovalves" as tri-leaflet heart valve-shaped tissues,[20,21] and "biocovered stents" as hybrid IVR devices,[22] have been developed. In this study, by shortening of the encupsulation period weak and ununiform wall structure was prepared particularly for observation of the variety of vascular graft fate. As expected, normal, stenosis, or aneurysm models were appropriately obtained in one rat.

The assessment of graft status using MR imaging does, however, have limitations. When using certain materials for artificial grafts (e.g., ePTFE and Dacron), MR imaging might be difficult owing to graft artifacts. Furthermore, such as ultrasound and/or digital subtraction angiography, it is difficult to evaluate blood stream by 3D evaluation. The TOF-MRA is more appropriate for the evaluation of tissue-engineered vascular grafts. The signal-to-noise ratio in image quality on TOF-MRA is strongly dependent on the static field strength and the coil design. Further study should be needed in developing coil. We hope that others who study at understanding the patho-physiological status and evaluating the efficacy/side effects of newly developed treatments, such as pharmaceutical and regenerative medicine.

CONCLUSIONS

Contrast-free TOF-MRA with 3-Tesla allowed an assessment of tissue-engineered small-caliber vascular graft status in the rat systemic arterial circulation. As the protocol used in this study is simple and noninvasive, it is useful for the longitudinal evaluation of graft status in the rat; this will contribute to enhancing the development of tissue-engineered small-caliber vascular grafts, particularly in the field of regenerative medicine.

REFERENCES

1. Tomizawa Y. Vascular prostheses for aortocoronary bypass grafting: A review. Artif Organs 1995;19:39–45.
2. Ferrari ER, Von Segesser LK. Arterial grafting for myocardial revascularization: How better is it? Curr Opin Cardiol 2006; 21:584–588.
3. Zilla P, Bezuidenhout D, Human P. Prosthetic vascular grafts: Wrong models, wrong questions and no healing. Biomaterials 2007;28:5007–5027.
4. Pasquinelli G, Freyrie A, Preda P, Curti T, D'addato M, Laschi R. Healing of posthetic arterial grafts. Scanning Microsc 1990;4:351–362.
5. Isenberg BC, Williams C, Tranquillo RT. Small-diameter artificial arteries engineered in vitro. Circ Res 2006;98:25–35.
6. Doi K, Nakayama Y, Oka T, Matsuda T. A new microporous polyurethane vascular graft prepared by an excimer laser ablation technique. ASAIO J 1995;41:M608–M611.
7. Campbell JH, Efendy JE, Campbell GR. Novel vascular graft grown within recipient's own peritoneal cavity. Circ Res 1999; 85:1173–1178.
8. Pektok E, Nottelet B, Tille JC, Gurny R, Kalangos A, Moeller M, Walpoth BH. Degradation and healing characteristics of small-diameter poly (epsilon-caprolactone) vascular grafts in the rat systemic arterial circulation. Circulation 2008;118:2563–2570.
9. Nakayama Y, Ishibashi-Ueda H, Takamizawa K. In vivo tissue-engineered small-caliber arterial graft prosthesis consisting of autologous tissue (Biotube). Cell Transplant 2004;13: 439–449.

10. Sakai O, Kanda K, Ishibashi-Ueda H, Takamizawa K, Ametani A, Yaku H, Nakayama Y. Development of the wing-attached rod for acceleration of "Biotube" vascular grafts fabrication in vivo. J Biomed Mater Res B Appl Biomater 2007; 83:240–247.
11. Watanabe T, Kanda K, Ishibashi-Ueda H, Yaku H, Nakayama Y. Development of biotube vascular grafts incorporating cuffs for easy implantation. J Artif Organs 2007;10:10–15.
12. Kempen DH, Yaszemski MJ, Heijink A, Hefferan TE, Creemers LB, Britson J, Maran A, Classic KL, Dhert WJ, Lu L. Non-invasive monitoring of BMP-2 retention and bone formation in composites for bone tissue engineering using SPECT/CT and scintillation probes. J Control Release 2009; 134:169–176.
13. Hobo K, Shimizu T, Sekine H, Shin'oka T, Okano T, Kurosawa H. Therapeutic angiogenesis using tissue engineered human smooth muscle cell sheets. Arterioscler Thromb Vasc Biol 2008;28:637–643.
14. Mccarthy I. The physiology of bone blood flow: A review. J Bone Joint Surg Am 2006;88:4–9.
15. Brockmann MA, Kemmling A, Groden C. Current issues and perspectives in small rodent magnetic resonance imaging using clinical MRI scanners. Methods 2007;43:79–87.
16. Yamamoto A, Sato H, Enmi J, Ishida K, Ose T, Kimura A, Fujiwara H, Watabe H, Hayashi T, Iida H. Use of a clinical MRI scanner for preclinical research on rats. Radiol Phys Technol 2009;2:13–21.
17. Smith DA, Clarke LP, Fiedler JA, Murtagh FR, Bonaroti EA, Sengstock GJ, Arendash GW. Use of a clinical MR scanner for imaging the rat. Brain Res Bull 1993;31:115–120.
18. Guzman R, Lövblad KO, Meyer M, Spenger C, Schroth G, Widmer HR. Imaging the rat brain on a 1.5 T clinical MR-scanner. J Neurosci Methods 2000;97:77–85.
19. Huang H, Zhou YM, Ishibashi-Ueda H, Takamizawa K, Ando J, Kanda K, Yaku H, Nakayama Y. *In vitro maturation* of "Biotube" vascular grafts induced by a 2-day pulsatile flow loading. J Biomed Mater Res B Appl Biomater 2009 [Epub ahead of print].
20. Hayashida K, Kanda K, Yaku H, Ando J, Nakayama Y. Development of an in vivo tissue-engineered, autologous heart valve (the biovalve): Preparation of a prototype model. J Thorac Cardiovasc Surg 2007;134:152–159.
21. Hayashida K, Kanda K, Oie T, Okamoto Y, Sakai O, Watanabe T, Ishibashi-Ueda H, Onoyama M, Tajikawa T, Ohba K, Yaku H, Nakayama Y. "In vivo tissue-engineered" valved conduit with designed molds and laser processed scaffold. J Cardiovasc Nurs 2008;23:61–64.
22. Nakayama Y, Zhou YM, Ishibashi-Ueda H. Development of in vivo tissue-engineered autologous tissue-covered stents (biocovered stents). J Artif Organs 2007;10:171–176.

Multicenter Evaluation of a Standardized Protocol for Rest and Acetazolamide Cerebral Blood Flow Assessment Using a Quantitative SPECT Reconstruction Program and Split-Dose ^{123}I-Iodoamphetamine

Hidehiro Iida[1,2], Jyoji Nakagawara[1,3], Kohei Hayashida[1,4], Kazuhito Fukushima[1,5], Hiroshi Watabe[1,2], Kazuhiro Koshino[1,2], Tsutomu Zeniya[1,2], and Stefan Eberl[1,6]

[1]Dual-Table Autoradiography SPECT Research Group in Japan, Osaka, Japan; [2]National Cerebral and Cardiovascular Center–Research Institute, Osaka, Japan; [3]Nakamura Memorial Hospital, Sapporo, Japan; [4]Takeda Hospital, Kyoto, Japan; [5]National Cerebral and Cardiovascular Center–Hospital, Osaka, Japan; and [6]Royal Prince Alfred Hospital, Sydney, Australia

SPECT can provide valuable diagnostic and treatment response information in large-scale multicenter clinical trials. However, SPECT has been limited in providing consistent quantitative functional parametric values across the centers, largely because of a lack of standardized procedures to correct for attenuation and scatter. Recently, a novel software package has been developed to reconstruct quantitative SPECT images and assess cerebral blood flow (CBF) at rest and after acetazolamide challenge from a single SPECT session. This study was aimed at validating this technique at different institutions with a variety of SPECT devices and imaging protocols. **Methods:** Twelve participating institutions obtained a series of SPECT scans on physical phantoms and clinical patients. The phantom experiments included the assessment of septal penetration for each collimator used and of the accuracy of the reconstructed images. Clinical studies were divided into 3 protocols, including intrainstitutional reproducibility, a comparison with PET, and rest–rest study consistency. The results from 46 successful studies were analyzed. **Results:** Activity concentration estimation (Bq/mL) in the reconstructed SPECT images of a uniform cylindric phantom showed an interinstitution variation of ±5.1%, with a systematic underestimation of concentration by 12.5%. CBF values were reproducible both at rest and after acetazolamide on the basis of repeated studies in the same patient (mean ± SD difference, −0.4 ± 5.2 mL/min/100 g, n = 44). CBF values were also consistent with those determined using PET (−6.1 ± 5.1 mL/min/100 g, n = 6). **Conclusion:** This study demonstrates that SPECT can quantitatively provide physiologic functional images of rest and acetazolamide challenge CBF, using a quantitative reconstruction software package.

Key Words: ^{123}I-iodoamphetamine; cerebral blood flow; acetazolamide; SPECT; vascular reactivity; quantitation

J Nucl Med 2010; 51:1624–1631
DOI: 10.2967/jnumed.110.078352

Received Apr. 27, 2010; revision accepted Jul. 14, 2010.
For correspondence or reprints contact: Hidehiro Iida, Department of Investigative Radiology, National Cerebral and Cardiovascular Center–Research Institute, 5-7-1 Suita City, Osaka 565-8565, Japan.
E-mail: iida@ri.ncvc.go.jp

Current clinical practice using SPECT relies largely on interpretation of qualitative images reflecting physiologic function. Quantitative functional parametric images may be obtained by applying mathematic modeling to SPECT data corrected for attenuation and scatter. Quantitative regional cerebral blood flow (CBF) (*1–3*) and cerebral vascular reactivity (CVR) in response to acetazolamide challenge (*4–6*) have been obtained with these techniques. One major application of such quantitative SPECT (QSPECT) approaches is the evaluation of ischemic status in patients with occlusion or stenosis in their middle cerebral arteries, to provide prognostic information of the outcome of revascularization therapies (*7*). Quantitative analysis in SPECT has also been demonstrated in the assessment of binding potential for several neuroreceptor ligands (*8,9*), for the quantitative assessment of regional myocardial perfusion (*10,11*), and for the assessment of radioaerosol deposition and clearance in healthy and diseased lungs (*12*). However, providing the standardized quantitative approach required for multicenter clinical trials has so far received only limited attention. Challenges remain in providing consistent quantitative data across institutions using a variety of SPECT equipment and vendor-specific reconstruction strategies (*13*). This limitation is attributed to a lack of standardized procedures in the reconstruction software offered by vendors, particularly in terms of correcting attenuation and scatter. Kinetic modeling for physiologic parameter estimation is also not part of the vendors' standard SPECT software. Although separate packages can be purchased for this purpose, they are not integrated and are flexible general-purpose packages, requiring considerable skill and knowledge to effectively use. Thus, they are not ideal for routine clinical use.

Scatter and attenuation occur in the object and are thus object-dependent but are not dependent on the geometry of the imaging equipment (*14*). Therefore, once a software program is developed to provide accurate image reconstruction with compensation for both attenuation and scatter, the

program should be able to provide quantitative images that are intrinsically independent of the geometric design of SPECT cameras. This is an attractive feature of SPECT for multicenter clinical studies.

From the various techniques available to correct for attenuation (*15*) and scatter (*16*), one feasible approach for clinical studies is based on a combination of attenuation correction, incorporated into the ordered-subset expectation maximization (OSEM) reconstruction (*17*), and scatter correction by the transmission-dependent convolution subtraction (TDCS) originally proposed by Meikle et al. (*18*). This approach has been extensively investigated by our group (*11,19*) for ^{99m}Tc for studies of the brain and heart (*18,20*) and also in cardiac ^{201}Tl studies (*11,21*). A recent study also demonstrated the accuracy of this approach in a combined SPECT/CT system (*22*). By incorporating a correction for collimator septal penetration by high-energy emissions, one can also make the technique applicable to ^{123}I (*19*).

The QSPECT reconstruction approach has estimated CBF images at rest in a clinical setting (*11*) and quantified CVR by measuring CBF at rest and after vasodilation in a single SPECT session. This was accomplished by using the dual-table autoradiographic (DTARG) method and a dual administration of ^{123}I-iodoamphetamine (*23*). In those studies, corrections for attenuation and scatter appeared to be essential for generating quantitative CBF maps that were consistent with those generated by ^{15}O-water PET (*11,23*).

These studies were, however, validated in a single institution using a limited range of SPECT systems, and the general applicability of this technique for different SPECT systems had yet to be fully established. Thus, the aim of this study was to verify that analysis of data with a standardized reconstruction package incorporating attenuation and scatter correction can provide reproducible results across multiple institutions for quantitative rest and acetazolamide challenge CBF estimation from a single SPECT session.

MATERIALS AND METHODS

Institutions and Subjects

The 12 participating institutions were clinical centers and generally did not have scientific staff dedicated to nuclear medicine software or hardware development. Standard, vendor-supplied software was used for the collection of the studies, with unmodified scanners and collimators clinically used for brain studies. The acquired data were reconstructed with the program package developed for this project. Manufacturers and models of camera systems and the number of detectors and collimators (including fanbeam or parallel hole) used by the institution are listed in Supplemental Table 1 (supplemental materials are available online only at http://jnm.snmjournals.org). All institutions performed experiments on physical phantoms according to the protocol described in the "Phantom Experiment" section. Of the 12 institutions, 9 obtained patient scans, whereas the remaining 3 provided only phantom data. Clinical studies were approved by institutions' ethics committees or followed guidelines for clinical research protocols authorized by the institution. All subjects at each institution gave written informed consent.

The clinical studies were divided into 3 protocols: intrainstitutional, intrasubject reproducibility (reproducibility); comparison with PET (vs. PET); and intrascan consistency of the dual-time-point split-dose (rest–rest). Studies were excluded from the analysis if there was severe patient motion during one of the studies or if there were changes in the condition of the patients between the first and second studies likely to lead to changes in CBF.

Eight institutions (institutions 1, 3, 4, 6, 8, 9, 11, and 12) participated in the reproducibility arm, in which quantitative CBF values measured on separate days were compared. In this arm, all patients experienced unilateral or bilateral stenosis or occlusion in the extracranial internal carotid artery. The patients' ages ranged from 43 to 81 y (mean ± SD, 65 ± 9 y). A total of 31 studies in this protocol were analyzed. Four patients had to be excluded from the analysis—2 because of significant changes in their pathophysiologic status between the studies and 2 because of severe motion and mispositioning in the scanner.

One institution (institution 4) performed the versus-PET studies. CBF values obtained by the DTARG method were compared with those by ^{15}O-water and PET. Studies were performed on 6 patients (5 men, 1 woman; age range, 71–74 y; mean age ± SD, 72 ± 1 y) with stenosis or occlusion of the extracranial internal carotid artery unilaterally (n = 3) or bilaterally (n = 3).

Two institutions (institutions 2 and 12) provided data for the rest–rest comparison. Five patients from institution 2 had chronic cerebral infarction, whereas 4 subjects from institution 12 had no sign of cerebral disease. Patients' ages ranged from 32 to 72 y (mean ± SD, 52 ± 15 y); 5 patients were men and 4 women.

Phantom Experiment

Three experiments were performed by each institution using the SPECT camera fitted with the collimators normally used in clinical brain studies. The first scan determined the absolute sensitivity or the becquerel calibration factor (BCF) of the reconstructed images. For 10 min, a 360° projection set was acquired of a syringe filled with a ^{123}I-iodoamphetamine solution of known radioactivity and placed at the center of the field of view. The syringe was supplied by Nihon-Medi Physics, and its radioactivity was calibrated to 111 MBq at noon on the day before the experiment, with an accuracy better than 3%, decaying to approximately 30 MBq at the time of the experiment, avoiding the dead time of the camera. The BCF was determined by dividing the absolute radioactivity by the total counts for the syringe region in the reconstructed image.

The second experiment determined the collimator septal penetration contribution (*24*) from high-energy photons into the primary 159-keV energy window for ^{123}I. A line-spread function was obtained from the projection data of a line source filled with ^{123}I-iodoamphetamine. The septal penetration was determined from the background level as described previously (*19*). A projection line-spread function was also generated from this line source placed in a water-filled cylindric phantom (diameter, 16 cm).

The third experiment used a 16-cm-diameter, 15-cm-long uniform cylindric phantom. The whole radioactivity used for the BCF determination was diluted into the phantom, and projection data were acquired for 30 min, using the clinical scan protocols described in the "Clinical Studies" section. The radioactivity concentration (counting rate per unit mass) of an approximately 0.3-mL sample from the phantom was measured using the well counters available at the various institutions. Both NaI- and plastic scintillator–based well counters were used (Supplemental Table

1). Average pixel counts derived from regions of interest on the reconstructed emission images were referred to the well counter radioactivity counting rate, to determine the cross-calibration factor between the SPECT images and well counter system. This cross-calibration factor was subsequently used for the blood sample counts of the clinical studies. Uniformity of the reconstructed emission images was evaluated.

Clinical Studies

All clinical SPECT studies followed the DTARG protocol, with dual administration of iodoamphetamine (*23*), depicted in Figure 1. Briefly, 2 dynamic scans were acquired in quick succession, with a 2-min interval between the scans. The first scan covered the initial 0- to 28-min period, and the second was acquired from 30 to 58 min. At 4 min per frame, 7 frames covered each of the 2 dynamic scan periods. ^{123}I-iodoamphetamine (111 MBq at institutions 2–12 or 167 MBq at institution 1) was infused twice over 1 min into the antecubital vein at 0 and 30 min. Acetazolamide (17 mg/kg, 1,000 mg maximum) was administered intravenously at 20 min after the first iodoamphetamine injection, corresponding to 10 min before the second iodoamphetamine injection. Projection data were summed for the acquisition duration of the first and second scans and reconstructed as described in the "QSPECT Reconstruction" section. In contrast to the study of Kim et al. (*23*), which used full arterial blood sampling, the individual arterial input functions were derived from a population-based standardized input function scaled with the whole-blood counts from a single arterial blood sample taken at approximately 10 min (*1,25–28*). This sample was also used for arterial blood gas analysis.

In the reproducibility arm, an additional, non-DTARG CBF study was performed on a separate day. Instead of DTARG, the previously reported ^{123}I-IMP autoradiographic (IMPARG) method (*1,19,25*) was performed within a month of the DTARG study. The IMPARG method is essentially equivalent to the present DTARG method, except that the IMPARG method uses a single iodoamphetamine administration to assess CBF either at rest or after acetazolamide challenge. The same image reconstruction process as for the DTARG protocol was used. In 12 studies, the DTARG protocol was used instead of IMPARG—namely, the DTARG study was performed twice to assess the CBF reproducibility at rest and after acetazolamide.

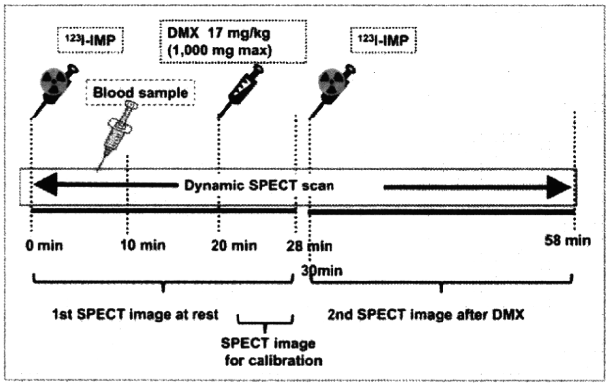

FIGURE 1. Scanning protocol flow for DTARG procedure. ^{123}I-iodoamphetamine was injected at 0 min, and 28-min resting dynamic SPECT scan was commenced. Blood sample for calibration of population input function was drawn at 10 min. Acetazolamide (DMX-diamox) was administered at 20 min. CBF values are scaled by last frame (time, 24–28 min). Second dynamic SPECT scan followed second injection of ^{123}I-iodoamphetamine at 30 min. IMP = iodoamphetamine.

In the versus-PET protocol, the PET study was performed within 2 d of the DTARG SPECT study. PET scans used intravenous ^{15}O-water both at rest and after the acetazolamide challenge. CBF images were calculated by the ^{15}O-water autoradiography technique (*29*), with careful corrections for delay and dispersion (*30–32*). Patients were stable between the SPECT and PET studies.

In the rest–rest protocol, the DTARG scan was obtained without the pharmacologic challenge during the study to evaluate the consistency of CBF values estimated from the 2 scans.

QSPECT Reconstruction

The program package for QSPECT uses a wrapper written in JAVA to run several programs written in C for Microsoft Windows systems. The package includes programs for reconstructing SPECT images, calculating functional images, coregistering images, and reslicing and printing summary logs.

The QSPECT package reconstructs images from the original projection data from commercial SPECT equipment, based on previous work by Iida and his colleagues (*19–21,23,33,34*). Reconstructed SPECT images are calibrated in Bq/mL, which provides independence from scanning parameters such as the acquisition time, number of views, matrix size, and zoom factor. Uniformity and center-of-rotation corrections and fanbeam–to–parallel beam conversion (for fanbeam collimators) were performed using the clinical routine software before reconstruction by this package.

An overall flow diagram of the correction and reconstruction process is shown in Supplemental Figure 1. The OSEM reconstruction technique includes attenuation correction (*17*). A threshold-based edge-detection algorithm generated the attenuation μ-map, assuming a uniform attenuation coefficient of 0.166 cm^{-1} for ^{99m}Tc (0.160 cm^{-1} for ^{123}I) as an average over the brain and skull (*19*). The threshold was optimized via the user interface to correctly define the brain outline. The attenuation μ-map was generated from the summed 0- to 28-min rest frame and was coregistered to the other images (*35*) reconstructed with filtered backprojection without attenuation or scatter correction. The attenuation μ-maps were forward projected to provide the transmission projection data for TDCS. The emission projections were scatter-corrected by the TDCS method, as originally proposed by Meikle et al. (*18*), and further optimized for realistic ^{99m}Tc, ^{201}Tl, and ^{123}I data in the brain and thorax regions (*20,21,23,33,34*). An offset compensated for the septal penetration of high-energy photons for ^{123}I studies, which adds fairly uniform background counts, or direct current (DC) components, to the projections.

Scatter- and attenuation-corrected images were reconstructed with OSEM (5 iterations, 5 subsets using geometric-mean projections, postreconstruction gaussian filter of 7 mm in full width at half maximum) and then realigned to the image set obtained from the first scan. The acquisition parameters and BCF were used to convert the reconstructed raw counts to Bq/mL.

The global CBF over the entire gray matter was estimated from the SPECT frame covering 24–28 min, because this timing minimizes the individual shape variations in individual input function. The look-up table generated for estimating CBF images from the complete dynamic study (0–28 min) was then

scaled to provide global cortical gray matter CBF values consistent with the 24- to 28-min frame estimates. A careful detection algorithm was used to reliably exclude extracranial accumulation of ^{123}I-iodoamphetamine (e.g., in the parotid region), which could adversely affect this scaling procedure. The regional CBF was then estimated at each pixel by means of the table look-up procedure (*25,28*). The background image at the time of the second ^{123}I-iodoamphetamine injection was estimated from the first-phase CBF images, according to the compartment model assumed in this study (*23*). An additional table look-up procedure was applied to the second dynamic dataset (30–58 min) for calculating the vasodilated (acetazolamide challenge) CBF images as described previously (*23*). The data were successfully reconstructed, and CBF was estimated at each institution. To facilitate and provide consistent analysis, the data presented are from the reanalysis conducted at the core lab (National Cerebral and Cardiovascular Center).

Data Analysis

The uniform phantom SPECT activity estimates were compared with the known activity in the phantom. Images for the baseline study were displayed with subsequent images using an absolute flow value scale to visually ascertain regional and global differences in flow. Regions of interest were placed on the middle cerebral artery territories of both hemispheres, and the average flow values between the different methods were compared and plotted. Bland–Altman plots and the SD of the differences evaluated the consistency of CBF values obtained from the reproducibility and versus-PET protocols.

All data were presented as mean ± SD. Pearson correlation analysis and linear regression analysis were used to evaluate relationships between the 2 CBF values. A P value less than 0.05 was considered statistically significant.

RESULTS

Phantom Studies

In the 16-cm scattering cylinder line source experiment, the scatter-uncorrected images show background counts extending beyond the phantom, from septal penetration of the high-energy photons. The scatter correction is largely effective in correcting for scatter and septal penetration counts. As shown in Supplemental Figure 2, the Toshiba-ECAM low- to medium-energy general-purpose (LMEGP) collimator, designed for reduced ^{123}I septal penetration, compared with the standard low-energy high-resolution collimator (GE Healthcare), demonstrates reduced scatter and septal penetration counts. The lower septal penetration of the Toshiba-ECAM LMEGP collimators is also supported by a lowered scatter correction offset value (DC = 0.05, compared with DC = 0.20 for the GE low-energy high-resolution collimator). The reduced scatter and septal penetration result in more complete removal of scatter for the LMEGP collimator.

Figure 2 displays reconstructed slices of the uniform phantom for all 12 institutions, scaled to the same maximum activity concentration. The estimated activity concentrations from these studies, compared with the known activity concentration, represented an accuracy of 87.5% ± 5.1% (Supplemental Table 1). The well counter–to–SPECT cross-calibration factor, which represents the sensitivity of the well counter system for ^{123}I, was 0.5–1.0 for NaI systems and 0.1–0.2 for plastic scintillation detector systems. The BCF values were consistent for the same SPECT camera–collimator configurations.

Clinical Studies

Figure 3A shows typical CBF images obtained at 4 institutions with 4 different γ-camera vendors, performed as part of the reproducibility arm of the study. Each case shows different CBF distributions both at rest and after acetazolamide challenge. The acetazolamide images obtained using the DTARG method agree well with the images subsequently obtained with the IMPARG method after acetazolamide infusion.

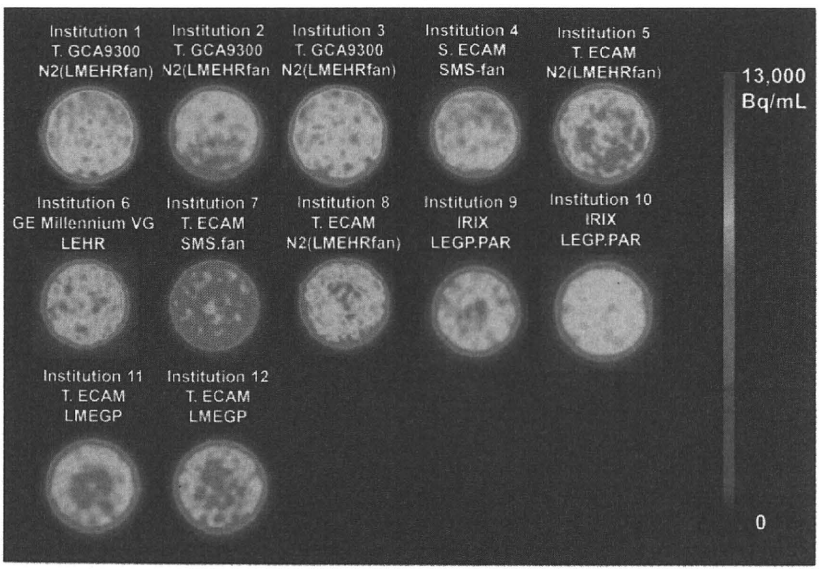

FIGURE 2. Reconstructed slices through uniform phantom from the participating 12 institutions. Experiment was designed to have same phantom activity concentration for each center's study. Nonuniformities and also differences in absolute activity concentration estimates can be observed, highlighting need for rigorous calibration, flood correction, and quality control. Legend above each image gives institution number (given in Supplemental Table 1), γ-camera model, and collimator used.

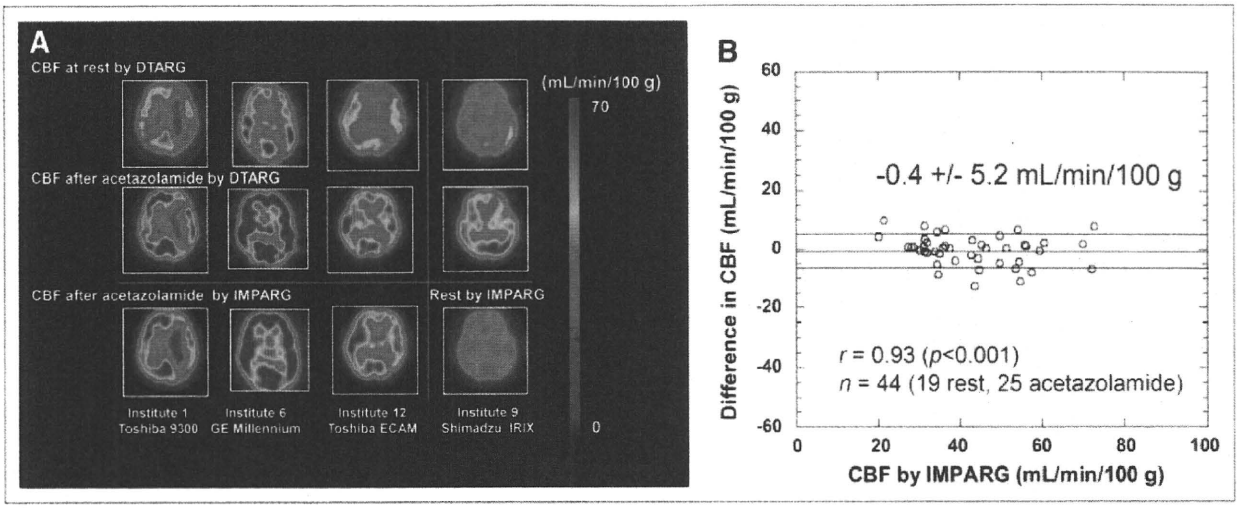

FIGURE 3. (A) Images from reproducibility study. CBF images obtained at rest and after acetazolamide with DTARG method. Repeated scan (third row) within 1 mo using IMPARG method and acetazolamide stress (columns 1–3) and at rest (last column). Images demonstrate that CVR can be estimated with this technique and demonstrate good reproducibility of measuring both at rest and after acetazolamide challenge CBF. (B) Bland–Altman plot showing difference vs. IMPARG CBF values estimated from DTARG method and repeated IMPARG studies to assess reproducibility. Little systematic bias is detected (mean difference, −0.4 mL/100 g/min), and SD of differences is moderate (5.2 mL/100 g/min). Correlation coefficient of $r = 0.93$ ($P < 0.001$) was found.

CBF images of a subject with left middle cerebral artery occlusion are shown in Supplemental Figure 3 for slices covering the whole brain. The images demonstrate reduced CBF after acetazolamide challenge in the left middle cerebral artery territory. The good reproducibility is confirmed by the Bland–Altman plot comparison of DTARG CBF values, with the CBF values obtained at a different imaging session with IMPARG or DTARG (Fig. 3B). The SD of the differences is 5.2 mL/100 g/min, with low bias supported by the mean difference of 0.4 mL/100 g/min. Regression analysis between DTARG and IMPARG values yielded a significant correlation ($P < 0.001$), with a correlation coefficient of $r = 0.93$.

Figure 4A shows MR and CBF images at rest and after acetazolamine obtained with DTARG SPECT and ^{15}O-water PET in a 73-y-old male patient (63 kg) with right internal carotid artery occlusion and left internal carotid stenosis. The MR images do not show any evidence of cerebral infarction in either hemisphere. Rest CBF was reduced bilaterally in the frontal-to-parietal regions, and acetazolamide increased CBF in left parietal regions but not in the right parietal area. DTARG CBF indicated the loss of vasoreactivity in the right internal carotid artery stenotic area. These findings were consistent with those from the PET evaluation. An additional example is shown in Supplemental Figure 4 for a 74-y-old female patient (48 kg) with left internal carotid artery stenosis, for whom MR images did not show cerebral infarction. DTARG CBF demonstrated preserved CBF in both hemispheres but reduced CBF reactivity in the left middle cerebral artery territory. The findings were again consistent with those from PET. Figure 4B compares the flow values obtained at rest and after acetazolamide with DTARG with the corresponding values obtained by ^{15}O-water PET. The SD of the differences is 5.1 mL/100 g/min, with the significant underestimation by ^{15}O-water PET, compared with PET by the DTARG method, highlighted by a mean difference of −6.1 mL/100 g/min. The Pearson analysis showed a significant correlation ($P < 0.001$), with a correlation coefficient of $r = 0.88$.

The results from the rest–rest protocol are summarized in Figure 5. The differences between the measurements performed with the 2 injections were small, with good agreement between the 2 flow values. The mean ± SD of the differences was 0.6 ± 2.9 mL/100 g/min.

DISCUSSION

The QSPECT package provided quantitative images consistent between the participating centers, using dual- or triple-detector SPECT scanners and collimators routinely used for nonquantitative brain studies. All centers successfully acquired the dynamic SPECT images, and the data from the variety of cameras encountered were successfully processed by the software package. Rest CBF and CVR could be readily obtained by the participating institutions in a single, clinically practical, 1-h scanning session. Good reproducibility of CBF estimates was observed in 31 pairs of studies at 8 institutions (Fig. 3), and the CBF estimated with the ^{123}I-iodoamphetamine SPECT agreed well with ^{15}O-water PET CBF at 1 institution (Fig. 4). The CBF values after the second injection of the DTARG were consistent with the values obtained after the

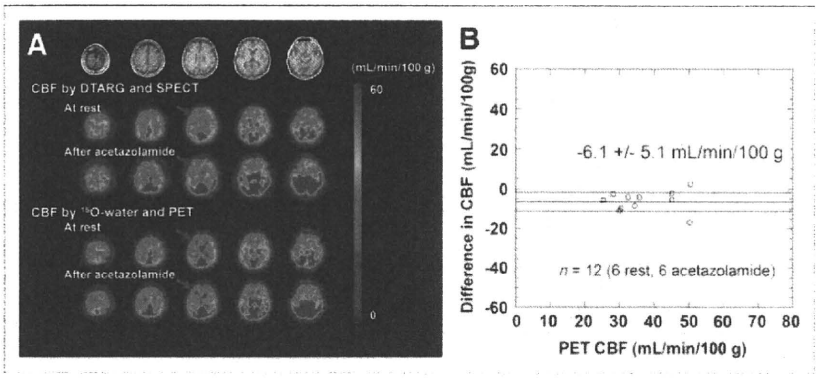

FIGURE 4. (A) MR and CBF images at rest and after acetazolamide stress assessed with corresponding measurements with ^{15}O-water PET (vs. PET evaluation) in patient with right internal carotid artery occlusion and left internal carotid stenosis. Gaussian filter was not applied to SPECT CBF in this display. (B) Bland–Altman plot. Moderate underestimation of CBF determined by DTARG method, compared with PET, is observed (mean difference, −6.1 mL/100 g/min). Correlation coefficient of $r = 0.88$ ($P < 0.001$) was found.

first injection when no vasodilating stress was given in 9 studies at 2 institutions (Fig. 5).

Quantitative CBF and CVR in response to acetazolamide challenge can be of significant prognostic value for patients considered for revascularization of cerebral arteries (*5–7*). The previously validated IMPARG method requires 2 independent scans on different days to assess the CVR (*5–7*), limiting it for routine clinical studies. The DTARG protocol to quantitatively assess CBF both at rest and after acetazolamide from a single dynamic SPECT session with the dual administration of ^{123}I-iodoamphetamine (*23*) facilitates clinical use. Errors caused by ambiguity in the absolute scaling, and possible changes in physiologic status of the subjects between scans, can be reduced substantially with the DTARG protocol. The quantitative reconstruction program enabled the compartment model–based kinetic analysis to compensate for the residual radioactivity concentration during the second session of the dynamic scan.

Major error sources in SPECT, namely attenuation and scatter, are only object-dependent (*14*) and not γ-camera– or collimator-dependent, and thus SPECT images obtained by this quantitative reconstruction package should be consistent across systems. Septal penetration of high-energy photons for ^{123}I is, however, collimator-dependent (*24*) but could be compensated as part of the TDCS scatter correction algorithm (*11*), as demonstrated in Supplemental Figure 2. The radioactivity concentration of the uniform cylinder phantom estimated in units of Bq/mL was consistent and showed variation within ±5.1% (Fig. 2; Supplemental Table 1), though a systematic underestimation by 12.5%, which is attributed to the BCFs being derived from a line source in air, reconstructed without scatter, attenuation, and septal penetration corrections. However, this underestimation does not affect the CBF estimation, because it relies on the direct cross-calibration between the γ-counter used to count the blood sample and the SPECT measurements.

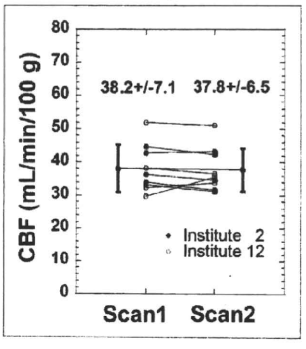

FIGURE 5. Results from rest–rest evaluation carried out at 2 institutions (2 and 12). In this study, DTARG method was performed as per normal protocol but without pharmacologic stress. CBFs estimated with first injection (left on graph) are in good agreement with those estimated after second injection (right on graph).

This phantom study also highlighted the importance of proper calibration and quality control of the γ-camera to avoid artifacts and bias in the reconstructed images. These corrections were applied, as for other clinical studies, by the vendors' software rather than as part of the QSPECT system, because these corrections are typically performed online and on-the-fly, with only the corrected data being stored. The nonuniformities seen on some phantom images should improve with more rigorous quality-control procedures.

The previously validated population-based input function requiring only a single arterial blood sample for scaling (*1,25–28*) has been incorporated in the software package. Blood from this single arterial sample is also used to measure arterial blood gases, which are relevant and of interest clinically in these patients. The timing of the single blood sample (~10 min after iodoamphetamine injection) was optimized previously (*1,25–28*) to minimize the errors associated with individual differences in shape of the arterial input function. In addition, absolute global CBF was estimated from SPECT images taken at an optimized mid scan time of approximately 30 min (24–28 min), rather than from the initial part of the study, to maximize the accuracy of using the population-based input function (*1,25–28*).

Partial-volume correction has not been implemented as part of this processing protocol. Partial-volume effects can potentially lead to underestimation of flow values in gray matter regions because of the limited resolution of SPECT. The small underestimation of 6.1 mL/100 g/min by the DTARG method, compared with ^{15}O-water PET (Fig. 4B), is attributed to the partial-volume effects due to differences in resolution between PET and SPECT. The underestimation can also lead to variations in CBF values obtained with different-

resolution collimators. However, consistent postreconstruction filtering, as applied in this study, can reduce this effect.

Only the reproducibility within an institution was assessed. Hence, the reproducibility of measurements between institutions cannot be gleaned from these data, particularly because patients with vascular disease were studied. Thus, unlike estimates from healthy volunteers, flow values and vascular reactivity are expected to vary from patient to patient, and flow values determined at one institution with one group of patients are therefore not directly comparable with flow values from another group of patients in another institution. A realistic brain phantom, such as recently developed by our group, simulating head contour with bone attenuation, could be used to assess the consistency of brain images between institutions.

CONCLUSION

The developed QSPECT package allows absolute CBF and CVR to be estimated in routine clinical studies. This multicenter study has demonstrated the applicability of QSPECT for a variety of clinical settings and equipment. Results from the studies suggest that a change of approximately 10% or 5 mL/min/100 g can be readily detected in follow-up studies. The graphical user interface for easily controlling the in-built sophisticated programs and tools ensures that routine use does not require dedicated support from scientific or computing staff. The package is now successfully used in over 130 institutions in Japan, and more than 25,000 patient studies have been analyzed with the QSPECT package.

ACKNOWLEDGMENTS

We thank the staff of each of the following institutions that participated in this project for their invaluable help with supporting the SPECT studies: Azabu Neurosurgical Hospital, Sapporo City; Asahikawa Red Cross Hospital, Asahikawa City; Handa City Hospital, Handa City; Ichinomiya Municipal Hospital, Ichinomiya City; Kashiwaba Neurosurgical Hospital, Sapporo City; Japanese Red Cross Kobe Hospital, Kobe City; Nakamura Memorial Hospital, Sapporo City; National Cardiovascular Center, Osaka; Ogori Daiichi General Hospital, Yamaguchi City; Oji General Hospital, Tomakomai City; Sunagawa City Medical Center, Sunagawa City; and Teine Keijinkai Hospital, Sapporo City. The present study was supported by the Japan Cardiovascular Research Foundation and a grant for Translational Research from the Ministry of Health, Labor and Welfare (MHLW), Japan.

REFERENCES

1. Iida H, Akutsu T, Endo K, et al. A multicenter validation of regional cerebral blood flow quantitation using [^{123}I]iodoamphetamine and single photon emission computed tomography. *J Cereb Blood Flow Metab.* 1996;16:781–793.
2. Hatazawa J, Iida H, Shimosegawa E, Sato T, Murakami M, Miura Y. Regional cerebral blood flow measurement with iodine-123-IMP autoradiography: normal values, reproducibility and sensitivity to hypoperfusion. *J Nucl Med.* 1997;38: 1102–1108.
3. Yamaguchi T, Kanno I, Uemura K, et al. Reduction in regional cerebral metabolic rate of oxygen during human aging. *Stroke.* 1986;17:1220–1228.
4. Ogasawara K, Ito H, Sasoh M, et al. Quantitative measurement of regional cerebrovascular reactivity to acetazolamide using ^{123}I-*N*-isopropyl-*p*-iodoamphetamine autoradiography with SPECT: validation study using $H_2{}^{15}O$ with PET. *J Nucl Med.* 2003;44:520–525.
5. Ogasawara K, Ogawa A, Terasaki K, Shimizu H, Tominaga T, Yoshimoto T. Use of cerebrovascular reactivity in patients with symptomatic major cerebral artery occlusion to predict 5-year outcome: comparison of xenon-133 and iodine-123-IMP single-photon emission computed tomography. *J Cereb Blood Flow Metab.* 2002;22:1142–1148.
6. Ogasawara K, Ogawa A, Yoshimoto T. Cerebrovascular reactivity to acetazolamide and outcome in patients with symptomatic internal carotid or middle cerebral artery occlusion: a xenon-133 single-photon emission computed tomography study. *Stroke.* 2002;33:1857–1862.
7. Ogasawara K, Ogawa A. JET study (Japanese EC-IC Bypass Trial) [in Japanese]. *Nippon Rinsho.* 2006;64(suppl 7):524–527.
8. Fujita M, Ichise M, Zoghbi SS, et al. Widespread decrease of nicotinic acetylcholine receptors in Parkinson's disease. *Ann Neurol.* 2006;59:174–177.
9. Deloar HM, Watabe H, Kudomi N, Kim KM, Aoi T, Iida H. Dependency of energy and spatial distributions of photons on edge of object in brain SPECT. *Ann Nucl Med.* 2003;17:99–106.
10. Iida H, Eberl S, Kim KM, et al. Absolute quantitation of myocardial blood flow with ^{201}Tl and dynamic SPECT in canine: optimisation and validation of kinetic modelling. *Eur J Nucl Med Mol Imaging.* 2008;35:896–905.
11. Iida H, Eberl S. Quantitative assessment of regional myocardial blood flow with thallium-201 and SPECT. *J Nucl Cardiol.* 1998;5:313–331.
12. Eberl S, Chan HK, Daviskas E, Constable C, Young I. Aerosol deposition and clearance measurement: a novel technique using dynamic SPET. *Eur J Nucl Med.* 2001;28:1365–1372.
13. Hapdey S, Soret M, Ferrer L. Quantification in SPECT: myth or reality? A multicentric study. *IEEE Nucl Sci Symp Conf Rec.* 2004;5:3170–3317.
14. Graham LS, Fahey FH, Madsen MT, van Aswegen A, Yester MV. Quantitation of SPECT performance: report of Task Group 4, Nuclear Medicine Committee. *Med Phys.* 1995;22:401–409.
15. Hendel RC, Corbett JR, Cullom SJ, DePuey EG, Garcia EV, Bateman TM. The value and practice of attenuation correction for myocardial perfusion SPECT imaging: a joint position statement from the American Society of Nuclear Cardiology and the Society of Nuclear Medicine. *J Nucl Cardiol.* 2002;9:135–143.
16. Zaidi H, Koral KF. Scatter modelling and compensation in emission tomography. *Eur J Nucl Med Mol Imaging.* 2004;31:761–782.
17. Hudson HM, Larkin RS. Accelerated image reconstruction using ordered subsets of projection data. *IEEE Trans Med Imaging.* 1994;13:601–609.
18. Meikle SR, Hutton BF, Bailey DL. A transmission-dependent method for scatter correction in SPECT. *J Nucl Med.* 1994;35:360–367.
19. Iida H, Narita Y, Kado H, et al. Effects of scatter and attenuation correction on quantitative assessment of regional cerebral blood flow with SPECT. *J Nucl Med.* 1998;39:181–189.
20. Narita Y, Eberl S, Iida H, et al. Monte Carlo and experimental evaluation of accuracy and noise properties of two scatter correction methods for SPECT. *Phys Med Biol.* 1996;41:2481–2496.
21. Narita Y, Iida H, Eberl S, Nakamura T. Monte Carlo evaluation of accuracy and noise properties of two scatter correction methods for ^{201}Tl cardiac SPECT. *IEEE Trans Nucl Sci.* 1997;44:2465–2472.
22. Willowson K, Bailey DL, Baldock C. Quantitative SPECT reconstruction using CT-derived corrections. *Phys Med Biol.* 2008;53:3099–3112.
23. Kim K, Watabe H, Hayashi T, et al. Quantitative mapping of basal and vasareactive cerebral blood flow using split-dose ^{123}I-idoamphetamine and single photon emission computed tomography. *Neuroimage.* 2006;33:1126–1135.
24. Kim KM, Watabe H, Shidahara M, Ishida Y, Iida H. SPECT collimator dependency of scatter and validation of transmission dependent scatter compensation methodologies. *IEEE Trans Nucl Sci.* 2001;48:689–696.
25. Iida H, Itoh H, Nakazawa M, et al. Quantitative mapping of regional cerebral blood flow using iodine-123-IMP and SPECT. *J Nucl Med.* 1994;35:2019–2030.
26. Iida H, Nakazawa M, Uemura K. Quantitation of regional cerebral blood flow using 123I-IMP from a single SPECT scan and a single blood sampling: analysis on statistical error source and optimal scan time [in Japanese]. *Kaku Igaku.* 1995; 32:263–270.
27. Kurisu R, Ogura T, Takikawa S, Saitō H, Nakazawa M, Iida H. Estimation and optimization of the use of standard arterial input function for split-dose administration of *N*-isopropyl-*p*[^{123}I]iodoamphetamine [in Japanese]. *Kaku Igaku.* 2002;39:13–20.

28. Ogura T, Takikawa S, Saito H, Nakazawa M, Shidahara M, Iida H. Validation and optimization of the use of standardized arterial input function in *N*-isopropyl-*p*[^{123}I]iodoamphetamine cerebral blood flow SPECT [in Japanese]. *Kaku Igaku.* 1999;36:879–890.
29. Shidahara M, Watabe H, Kim KM, et al. Evaluation of a commercial PET tomograph-based system for the quantitative assessment of rCBF, rOEF and $rCMRO_2$ by using sequential administration of ^{15}O-labeled compounds. *Ann Nucl Med.* 2002;16:317–327.
30. Iida H, Higano S, Tomura N, et al. Evaluation of regional differences of tracer appearance time in cerebral tissues using [^{15}O] water and dynamic positron emission tomography. *J Cereb Blood Flow Metab.* 1988;8:285–288.
31. Iida H, Kanno I, Miura S, Murakami M, Takahashi K, Uemura K. Error analysis of a quantitative cerebral blood flow measurement using $H_2{}^{15}O$ autoradiography and positron emission tomography, with respect to the dispersion of the input function. *J Cereb Blood Flow Metab.* 1986;6:536–545.
32. Iida H, Kanno I, Miura S, Murakami M, Takahashi K, Uemura K. A determination of the regional brain/blood partition coefficient of water using dynamic positron emission tomography. *J Cereb Blood Flow Metab.* 1989;9:874–885.
33. Iida H, Shoji Y, Sugawara S, et al. Design and experimental validation of a quantitative myocardial ^{201}Tl SPECT System. *IEEE Trans Nucl Sci.* 1999;46:720–726.
34. Narita Y, Iida H. Scatter correction in myocardial thallium SPECT: needs for optimization of energy window settings in the energy window-based scatter correction techniques [in Japanese]. *Kaku Igaku.* 1999;36:83–90.
35. Eberl S, Kanno I, Fulton RR, Ryan A, Hutton BF, Fulham MJ. Automated interstudy image registration technique for SPECT and PET. *J Nucl Med.* 1996;37:137–145.

特集 ここまできた神経画像

核医学的測定法の進歩

飯田秀博，銭谷 勉，越野一博，平野祥之
IIDA Hidehiro, ZENIYA Tsutomu, KOSHINO Kazuhiro, HIRANO Yoshiyuki
国立循環器病センター研究所・先進医工学センター　放射線医学部

PET 装置は検出器の精細化で空間解像度の上昇が進み，立体撮像によって高感度化が実現した．SPECT においては吸収と散乱線を正確に補正する画像再構成プログラムの利用によって，定量化と標準化が可能になった．このようななかで，従来よりも一歩踏み込んだ脳神経核医学画像の定量評価が可能になる．複数モダリティイメージングに加えて，調節機能などの診断は今後の課題である．

Key Words
機能画像，マルチモダリティ，マルチトレーサ，時間解像度

はじめに

PET が誕生してから 30 年以上の技術蓄積の結果，検出器の改良は空間解像度の一桁向上に，多断層化と立体計測技術の普及は感度の二桁上昇に貢献した．SPECT においては複数検出器やコリメータの進歩，さらに画像再構成理論の改善によって定量精度改善がなされた．複数モダリティの融合画像処理技術や，新しい画像再構成理論の整備と実用化も進み，神経画像の高精細化に貢献する．本稿では，新しい要素技術とその効果について概説する．

1　PET

PET 装置の空間解像度を決定するのはシンチレーション結晶の大きさであり，小型ブロック検出器の開発が高解像度化に貢献してきた．深さ情報（depth-of-interaction：DOI）を検出する検出器も実用化された．立体計測（三次元，3D）は完全に定着し測定感度は大きく改善し，1%を超えるに至った．臨床 PET 装置の空間解像度は概ね 4 mm 程度にまで向上した．画像再構成プログラムはさらに改良が進み，吸収補正や散乱線補正に加えて空間解像度の補正がなされるようになり，空間解像度は 2 mm 程度になったとされる．高性能な放射線検出シンチレータの実用化がなされ，また同時計測の時間分解能（coincidence window）が短くなった．これは画質劣化の最大の要因であった偶発同時計数の減少に貢献する．一部のメーカーでは time-of-flight 処理（同時計測信号の時間差より線源の場所を限局する機構）も搭載される．

現在の課題は，膨大な情報の高速処理技術の開発にあるといえる．PET では検出器総数の自乗に比例した計測線（line-of-response：LOR）の信号を扱う．典型的には

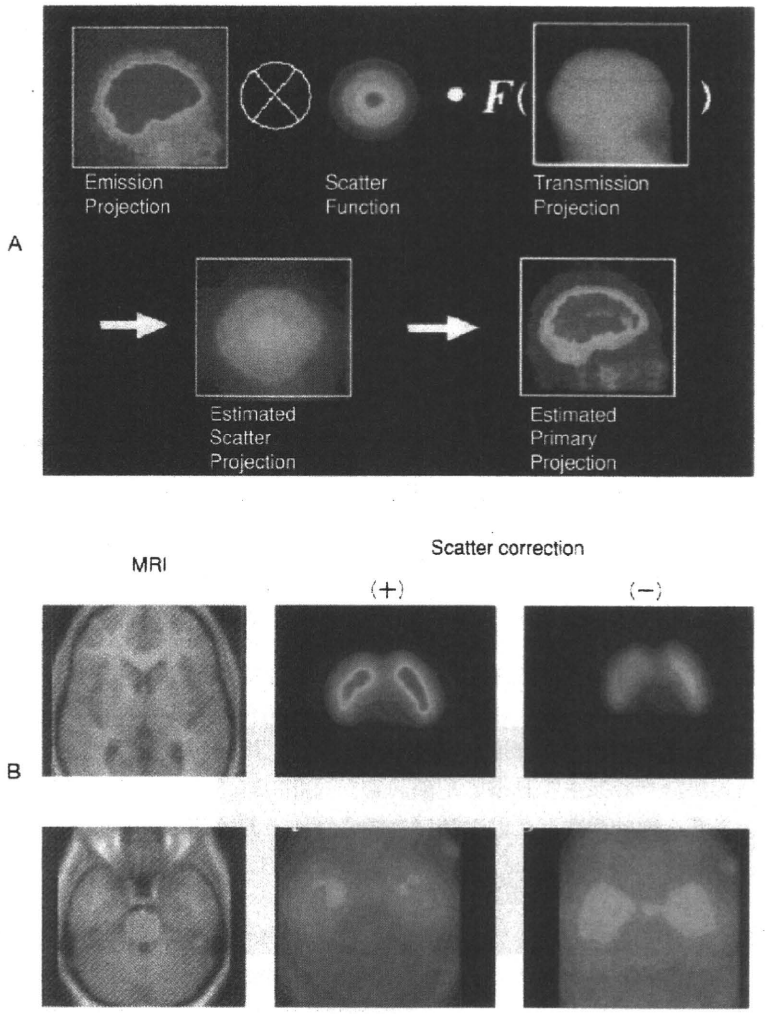

図❶ 定量的 SPECT 画像再構成における散乱線補正の効果
（A：Iida H *et al*, 1998[2]，B：Fujita M *et al*, 2004[4]より引用）
A：散乱線補正法の例．吸収減弱プロジェクションを利用した方法はノイズの高揚がなく良好な画像を提示する．B：I-123 標識 epidepride の結合能画像における散乱線補正の効果．散乱線補正は画像のコントラストを上昇させ，定量解析には不可欠である．

10^8にもなる LOR 信号を演算処理・保存するためには相当高速な電子回路を含む処理技術が必要である．また，3D PET 計測における散乱線を補正する普遍的な方法も確立されなければいけない．放射線分布と吸収減弱（μ）分布に物理公式（Klein-Nishina の式など）を適用する方法が提案されているが，視野外の放射能や散乱線発生の影響は意外に少ないことが当該研究グループ平野らによって明らかにされ，この方法の妥当性，また視野シールドの有効性が確認されたところである．いずれにせよ神経イメージングに向けた PET 計測技術は着実に進んでおり，さらに明瞭かつ高精度な画像の撮像が可能になる．

2 SPECT

SPECT 技術の最近の重要な進展は，定量化と標準化に向けた活動であろう．SPECT 画像の定量精度の確保は困難とされてきたが，吸収と散乱線を比較的正確に補正する実用的なプログラムの整備によって，メーカーや機種を超えた再現性が得られるようになった．これは施設を